AERODYNAMIC INVESTIGATION OF THE TIP SECTION FOR TITANIUM BLADE 54”

M. Luxa – D. Šimurda
Institute of Thermomechanics AS CR, v.v.i., Prague, Czech Republic
luxa@it.cas.cz, simurda@it.cas.cz

J.Fořt - J.Fürst - P. Šafařík
Faculty of Mechanical Engeneering, Czech Technical University in Prague, Prague, Czech Republic
jaroslav.fort@ fs.cvut.cz , jiri.furst@fs.cvut.cz, pavel.safarik@fs.cvut.cz

J. Synáč – B. Rudas
R&D Dept., Doosan Skoda Power, LTD., Pilsen, Czech Republic
jaroslav.synac@doosan.com, bartolomej.rudas@doosan.com

ABSTRACT

This paper presents an aerodynamic experimental and numerical investigation of the prismatic blade cascade that represents the tip section of a rotor comprising 52 titanium blades 1375mm in length. This rotor is designed for the last stage of the low pressure cylinder of a large output steam turbine. The flow conditions of the tip section are defined by the structural and operational demands in the last stage. The tip section is characterized by a supersonic inlet, a large stagger angle and a supersonic outlet. The profile applied to the tip section is relatively very thin, and its central line is unusually cambered, so the shapes of the suction and pressure sides have converse curvatures. The results of the aerodynamic experiments are compared with the results of numerical simulations calculated by both a commercial code and an in-house code.

NOMENCLATURE

b	[m]	chord of airfoil
b_{ax}	[m]	axial chord of airfoil
c_p	[J/kgK]	const. pressure specific heat
s	[m]	cascade pitch
t	[m]	max. thickness of airfoil
o	[m]	throat opening
p	[Pa]	pressure
x	[m]	coordinate
y	[m]	coordinate
M	[-]	Mach number
M^*	[-]	non-dimensional velocity
Mm	[kg/kmol]	molecular mass
Re	[-]	Reynolds number (related to the profile chord *b* and exit Mach number M_2 or M_{2is})
β	[deg]	velocity angle
ι	[deg]	incidence angle
γ	[deg]	stagger angle
λ	[W/mK]	heat conductivity
η	[Pa s]	viscosity
ρ	[kg/m^3]	specific mass
ζ	[-]	kinetic energy loss
κ	[-]	ratio of heat capacities

Subscripts

ax	axial direction
1,2	upstream resp. downstream cascade
is	isentropic
s	static value
t	total value
nom	nominal
1200	design point

OPEN ACCESS
Downloaded from www.euroturbo.eu
Copyright © by the Authors

INTRODUCTION

The efficiency of a steam turbine can be improved and the production costs can be reduced by increasing the exit area downstream the low pressure cylinders. A large exit area results in lower losses due to decreased exit velocity. Increasing the exit area also leads to a lower number of turbine flows and thus to lower production costs. An integral part of these endeavours is the need to design new, longer rotor blades for the last stage. The 1375mm titanium blade is typical example of efforts of this kind (Fig.1).

The relatively narrow space for the aerodynamic design of long blades often results in blades with tips operating under supersonic regimes. The peripheral speed of the titanium blade tip investigated here is approximately 740 ms^{-1} at 50 revolutions per second. An analysis of the velocity triangles shows clearly that the inlet and outlet velocities are much higher than the speed of sound. The stagger angle of the tip section profiles is very large, and the convergent - divergent tip profile cascade is designed for a very small flow turning angle. The fan of these long airfoils is highly opened on the tip diameter (the tip section will rotate on a diameter of 4700mm), so the overlapping of the adjacent profiles is very small (Fig.2).

The profile applied to the tip section (Fig.3) is relatively very thin, and its central line is unusually cambered, so the shapes of the suction and pressure sides have converse curvatures: the nature of the shape of the suction side is therefore concave and, conversely, the shape of the pressure side has a convex character. The rather complicated designing of profiles of this type is described e.g. by Senoo (2012).

The transonic flow through this type of cascade is very complex, and is also sensitive to relatively small changes in the parameters. We can therefore also expect the influence of some details in the algorithms implemented in the computational method. There is also a lack of experience with numerical solutions of the flow past turbine cascades with a supersonic inlet flow. It is very important to compare the results achieved using commercial software and widely used (and consequently validated) numerical algorithms with the results using in-house software, where there is complete knowledge of the numerical method, so that appropriate changes can be made to the algorithms.

The experimental investigation of the flow in this profile cascade is focused not only on the flow condition of the cascade operation point, but also on a wide range of off-design regimes. This attitude provides more information that will help us to understand the behaviour and the nature of basic phenomena occurring in the profile cascade flow field. The data from mutually independent optical and pneumatic measurements also make a significant contribution to our understanding.

Figure 1: **The titanium rotor blade 1375mm (54")**

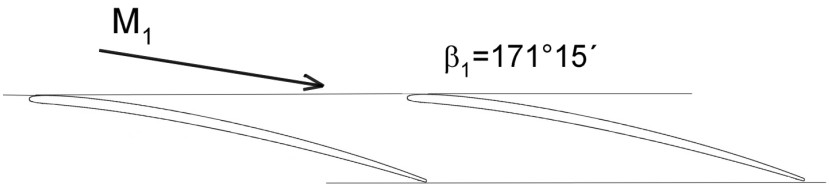

Figure 2: **The convergent-divergent tip profile cascade**

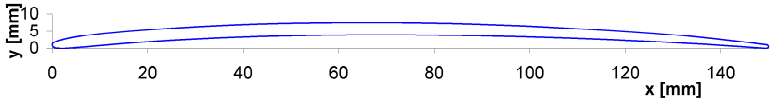

Figure 3: **Profile of the measured cascade**

Important integral flow characteristics (pressure forces, pressure loss, energy loss, exit flow angle, etc.) were also determined. However, if we concentrate on these integral characteristics only

(without making an effort to understand the nature of their origin and development), we will be limited to a utilitarian Heidegger technoscience attitude (Aronowitz et al. (1996)), which should not be the only aim of research workers.

EXPERIMENTAL FACILITY AND EXPERIMENTAL PROCEDURE

The profile cascade, which represents the tip section of the 1375 mm (54") long titanium rotor blade, consists of 8 prismatic blades only. The profile chord of the model was chosen b = 0.15m, i.e. the reduction scale is approximately 1:2, considering the real blade dimensions. The blade height is l = 0.16m, so the aspect ratio is AR = 1.07 only. The model dimensions result from many requirements and restrictions (e.g.: corresponding Reynolds number values, solidity of the blades, dimensions of the test section, etc.). The low value of the aspect ratio has negative effects on the 2D flow field parameters. The Axial Velocity Density Ratio (*AVDR*), which to some extent characterises the extent of 3D phenomena, was monitored during the pneumatic measurements; the *AVDR* values are plotted against the isentropic exit Mach number M_{2is} for different inlet Mach numbers M_1 in Fig. 4.

Two static pressure taps (0.8mm in diameter) are situated in the middle of the height of the blade and the profile chord on the blades which form the boundary of the middle channel of the cascade (one tap, p_{LH}, is on the pressure side; the other, p_{LD}, is on the suction side of the neighbouring profile (depicted in Fig. 8). The data from these two pressure taps provide information necessary for an evaluation of the interferograms.

The basic geometry and the characteristic dimensions of the profile cascade are shown in Table 1. The cascade will be operated under two nominal conditions: firstly, in a 1200 MW steam turbine for a nuclear power plant in Czech Republic and, secondly, in a 800MW steam turbine for a power plant in India. The nominal conditions for the two turbines are summarised in Table 2.

Table 1: **Characteristic dimensions of the blade cascade**

Pitch/Chord	s/b	0.951	Stagger Angle	γ	78.37°
Max. Thickness/Chord	t/b	0.025	Trailing Edge Thickness / Chord	t_{TE}/b	0.0033
Aspect Ratio	AR	1.07	Design Inlet Flow Angle	β_{1des}	171.25°
Throat Opening/Chord	o/b	0.169	Design Incidence	ι_{des}	0°

Table 2: **Operation condition of the tip section (in the steam)**

Turbine	M_1[-]	M_{2is}[-]	Re[-]
800 MW	1.46	1.768	$1.5 .10^6$
1200 MW	1.46	2.045	$1.1 .10^6$

The Reynolds number related to the profile chord b and to the isentropic exit Mach number M_{2is} in the wind tunnel (dry air) ranges from $Re = 1.02.10^6$ to $Re = 2.34.10^6$.

The experiments were carried out in the aerodynamic laboratory at Novy Knin. The high-speed intermittent blow-down wind tunnel for 2D cascade testing was used, and the flow medium was dry air. A special test section was used for an investigation of the flow in a prismatic profile cascade with a small flow turning angle and supersonic inlet velocity. This test section has been described by Matějka et al. (2013).

The high-speed wind tunnel for 2D cascade measurements (see Fig. 5) is equipped with an adjustable supersonic inlet nozzle. The nozzle has parallel side walls and the shape of the upper and lower wall can be continuously changed, so an inlet Mach number up to $M_1 = 2.0$ can be reached. The air flows from the test section to the settling chamber. The backpressure is controlled by an adjustable control nozzle, which is situated downstream the settling chamber. The scheme of the test section is depicted in Fig. 7. Both the upper wall and the lower wall of the inlet channel are equipped with perforated inserts. These inserts are connected to the low pressure parts of the wind

tunnel, and the suction is controlled by slide valves. The suction mode of the lower perforated wall is used for inlet velocities around a value of $M_1 = 1.0$, to improve the periodicity of the cascade inlet

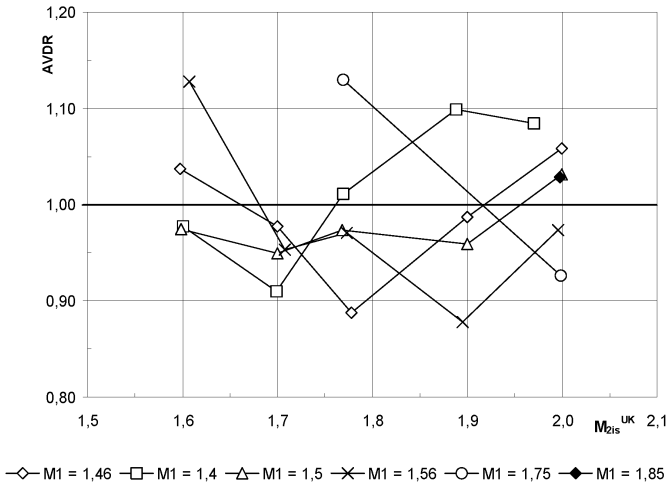

Figure 4: **The Axial Velocity Density Ratio (AVDR)**

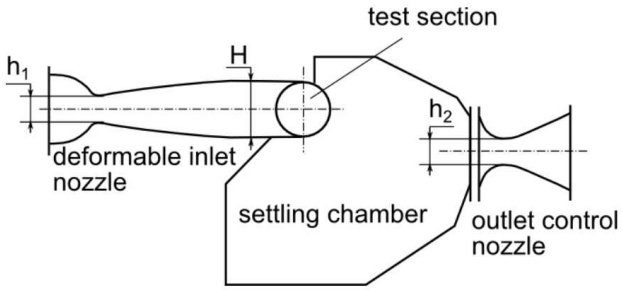

Figure 5: **Scheme of the suction type high-speed aerodynamic wind tunnel for 2D cascade measurements**

flow field. The upper perforated wall (with suction or with ventilation only) effectively prevents reflection of the outer branch of the inlet shock waves back into the studied flow field in the whole range of supersonic inlet Mach numbers, i.e. for $1 < M_1 < 2$. An example of the inlet isentropic Mach number distribution along approximately two pitches is shown in Fig. 6 (the positions of the static pressure taps are shown in Fig. 9).

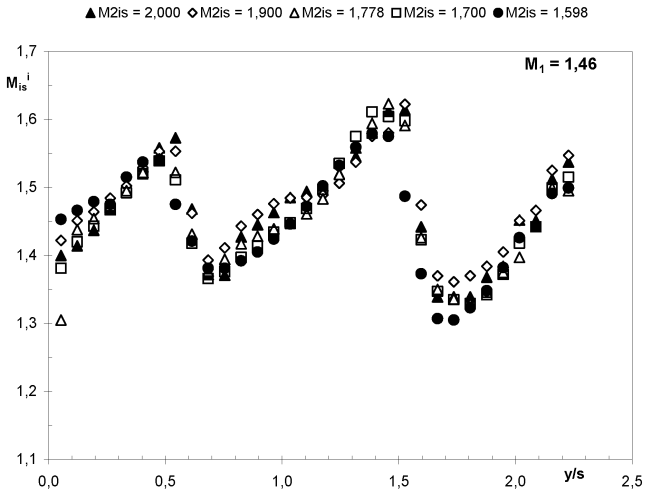

Figure 6: **An example of the isentropic Mach number distribution along two pitches upstream the cascade for supersonic inlet velocity**

The adjustable perforated tailboard is usually placed next to the trailing edge of the lateral profile in order to improve the periodicity of the exit flow field. In this specific configuration, the perforated tailboard is situated downstream the blade next to the lateral blade. The optimal value for the angle between the tailboard and the plane of the trailing edges of the cascade was found experimentally. The tailboard not only prevents exit shock waves from reflecting back to the exit flow field, it also prevents expansion taking place at the lower wall block edge from influencing the exit flow field (Šimurda et al. (2014)).

The inlet flow field parameters are measured by a number of static pressure taps on the sidewalls and by a Prandtl probe, which was placed upstream the cascade inlet. The relatively remote position of the probe is aimed at reducing the probe disturbances in the proximity of the leading edges of the cascade. The representative value of the inlet Mach number is evaluated from the average value of the static pressures, which is obtained from five pressure taps $p_{S2} \div p_{s6}$ (see Fig. 9) and the total pressure at the inlet (measured by the Prandtl probe), respectively. The isentropic exit Mach number was determined according to the static pressure, which was measured in the settling chamber downstream the cascade.

Optical measurements were carried out (interferometry – infinite fringe method, schlieren method in the Toepler configuration). The field of vision for the optical measurements covered an

important part of the cascade middle channel only (see Fig. 8). The dimension of this optical field is limited by the diameter of the glass windows for interferometry (180 mm).

The pneumatic measurements included a 2D traversing measurement downstream the cascade and a measurement of the static pressure distribution at the cascade inlet and outlet (see Fig. 9). The static pressure distribution was measured along two pitches near the leading edges and also along two pitches near the plane of the trailing edges by 64 static pressure taps on the sidewall of the test

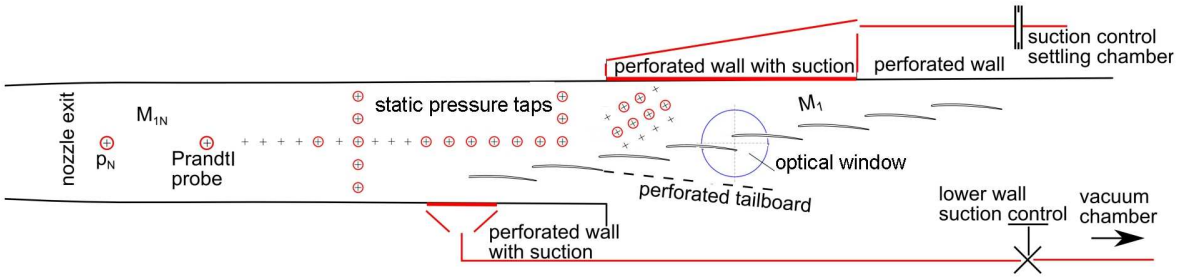

Figure 7: **Test section for an investigation of the flow in a prismatic profile cascade with a small flow turning angle and supersonic inlet velocity; arrangement for optical measurements**

section.

2D traversing measurements were made. The distributions of the static and total pressure and exit flow angle were measured using a conical five-hole probe (3.5mm in diameter in its cylindrical part) which traversed continuously along the straight path in the middle of the blade height 25mm behind the trailing edges. The PID controller automatically positions the traversing probe in the direction of the exit velocity vector. The probe traversed along one cascade pitch.

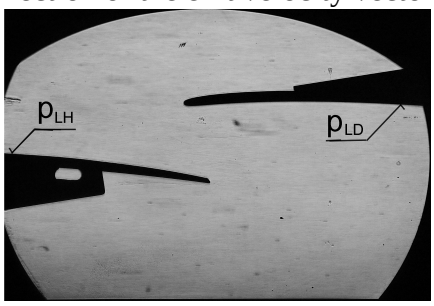

Figure 8: **The field of vision for the optical measurements**

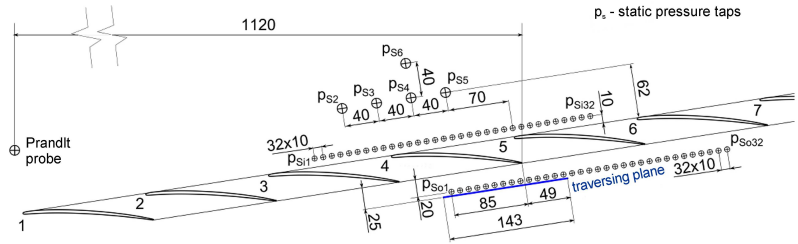

Figure 9: **Arrangement of the test section for the pneumatic measurements**

All traversing measurements were performed only once, and the repeatability of the measurements was not evaluated. The accuracy of the measuring equipment (traversing) enabled us to measure the kinetic energy loss coefficient ζ and exit flow angle β_2 with absolute uncertainties less than 0.004 and 2°, respectively.

During the experiments with supersonic inlet velocity, the profile cascade was fixed in the test section in the position corresponding to nominal flow conditions ($\iota = 0°$). The inlet flow angle at supersonic inlet Mach numbers was then set spontaneously due to the unique incidence rule (see for example Luxa et al. (2014)), which defines the unique relation between inlet Mach number and inlet flow angle. The unique incidence rule states that it is impossible to choose any inlet condition with respect to the inlet flow angle and the inlet Mach number. The value of the incidence angle corresponding to a particular inlet Mach number is dependent on the cascade geometry only, and it can be determined indirectly (methods of characteristics, CFD methods). The stagnation point shift, which corresponds to the incidence angle, cannot be determined experimentally, because the dimension of the leading edge of the tip profile is too small. Good information about the sensitivity

of the incidence angle to the inlet Mach number for different cascade layouts is given e.g. by Starken (1986). The position of the blade cascade in the test section was changed only at positive incidence ι = +3, at which the inlet Mach number was subsonic.

The optical and traversing measurements were carried out in practically the same range of velocities, i.e. $0.8 \leq M_{2is} \leq 2.0$ and $0.7 \leq M_1 \leq 1.85$. The geometrical incidence angle ι = 0° was set in cases with $M_1 \geq 1$ and $\iota = +3°$ for a subsonic inlet.

The evaluation of the interferograms is based on the principle of the interferometric methods (see Šafařík et al. (2000)) (the fringes in the flow field represent lines with a constant refraction index), and is also based on the assumption of isentropic changes in the main flow and constant static pressure across the boundary layer.

The loss coefficient ζ defined by relation (1) and the exit flow reference values were evaluated using the data reduction method, which is based on solving all the conservation laws (mass, momentum, energy), the equation of state for an ideal gas and the condition of adiabatic flow (see Amecke & Šafařík (1995)).

$$\zeta = 1 - \frac{M_2^{*2}}{M_{2is}^{*2}} \tag{1}$$

The non-dimensional velocity M^* (or the so-called characteristic Mach number M^*) is defined as the ratio of flow velocity w and the critical speed of sound a^* (the speed of sound at Mach number $M = 1$).

NUMERICAL SIMULATION

Two computational fluid dynamics methods were used. The computations carried out using commercial software cover the field of inlet Mach numbers in the range from $M_1 = 0.6$ to $M_1 = 1.9$ for isentropic exit Mach numbers $M_{2is} = 1.77$ and $M_{2is} = 2.05$ (outlet operation conditions). The computations using the in-house code were focused on three regimes, comprising three different inlet supersonic velocities at the invariant isentropic exit Mach number $M_{2is} = 1.77$.

Commercial Software

The calculations were performed using the commercial *Ansys Fluent* code, version 13.0. The *Fluent* code solves the system of governing equations numerically, using the finite volume method.

Table 3: **Ideal gas characteristics**

ρ	[kg.m^{-3}]	from ideal gas equation
c_p	[J.kg^{-1}.K^{-1}]	6533.6
λ	[W.m^{-1}.K^{-1}]	0.02298
η	[kg.m^{-1}.s^{-1}]	1.107.10^{-5}
κ	[-]	1.07
Mm	[kg.kmol^{-1}]	19.363

A 2D model of the investigated geometry was generated in *GridPro* the preprocessor, where the calculation domain was meshed with quadrilateral cells. The computational domain included areas of the flow field approximately one pitch upstream and downstream the cascade. The domain is shown in Fig. 10 (the evaluation planes are marked downstream and upstream the cascade). The grid quality was measured by equiangle skew. The 2D grid consisted of 135 964 cells. Only 5.3% of the cells exhibited a skew value above 0.7, while the maximal skew value was 0.8. A detail of the cells around the trailing edge is shown in Fig. 11. In the near wall region, the original mesh was fine enough ($y^+ < 0{,}4$) for a low-Reynolds turbulence model to be used, and no grid adaptation was necessary. The numerical results show that the changes in the loss coefficient are sensitive to the position of the evaluation plane downstream the cascade (see Fig. 12). A shift of the evaluation plane by a half of the pitch changes the loss coefficient by about 0.6%. The sensitivity of the value of the exit angle in relation to the position of the evaluation plane is lower (by about 0.3° of the exit angle value). The dependence of the inlet Mach number - evaluation plane position is depicted in Fig. 13.

The problem was solved using the density based implicit solver with Menter's *k-ω SST* model of turbulence. The flowing medium was wet steam, which was considered as an ideal gas, and its

characteristics are presented in Table 3. The inlet boundary conditions were determined by the constant total pressure, the total temperature and the inlet flow angle. The outlet boundary condition was defined as a constant static pressure. Periodicity conditions were applied to corresponding free side boundaries of the computation domain. A non-reflecting boundary condition was applied where appropriate.

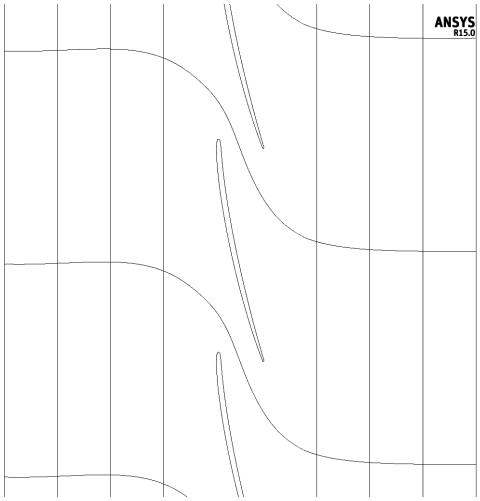

Figure 10: **The computational domain**

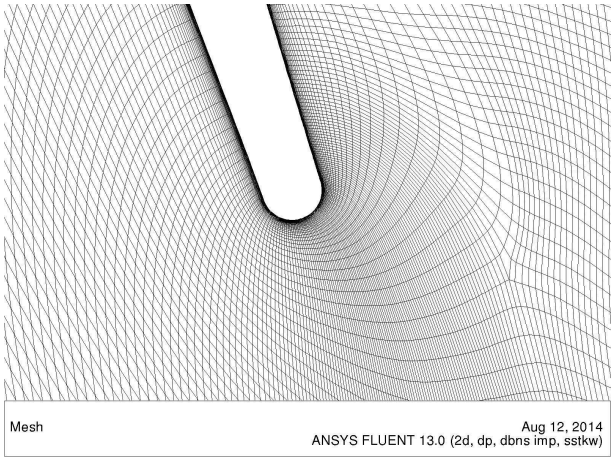

Figure 11: **Detail of the mesh around the trailing edge**

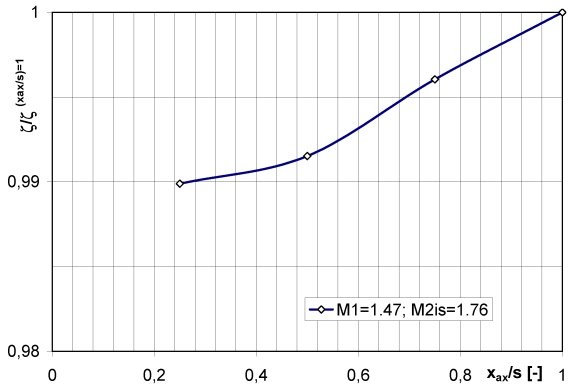

Figure 12: **Dependence of the loss coefficient on the position of the evaluation plane downstream the cascade (CFD -commercial code)**

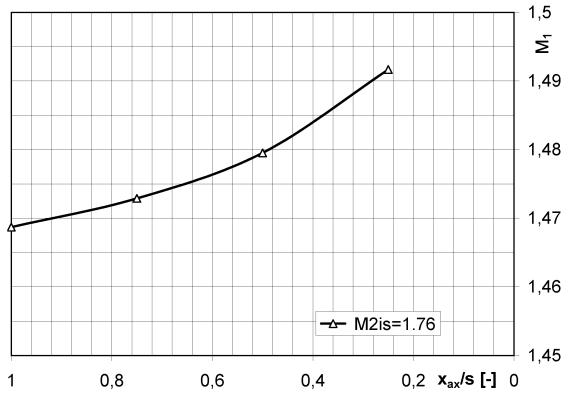

Figure 13: **Dependence of the inlet Mach number on the position of the evaluation plane upstream the cascade (CFD - commercial code)**

In-house Code

The 2D system of averaged Navier-Stokes equations together with the two equation *k-ω* SST model was solved using the in-house finite volume software, see Louda et al. (2012). This software was developed for calculations on a multi-block structured quadrilateral grid (2D version), and was used with the AUSM+up scheme, a linear 1D reconstruction on a finite volume with the van Leer limiter for convective terms and a central finite volume approximation of the dissipative terms. The implicit scheme was used for time evolution together with the block SLOR iterative solution of the system of linear equations. The computations were performed with the *k-ω* SST turbulence model with the Medic-Durbin limiter.

The computational domain consists of one pitch of the cascade. The inlet (outlet) boundary is located at an axial distance of about two (one) profile chords from the profile for the in-house software. Note that the simulation with commercial software was carried out using a shorter upstream part. We prescribe values for total pressure, total density and the velocity angle on the

inlet and static pressure on the outlet boundary. We then prescribe a non-slip condition and a no heat exchange condition on the surface of the profile surface and a periodicity condition on the periodic boundaries. In the numerical method, the constants in the inlet and outlet boundary conditions are considered as mean values of the variables along the corresponding boundary. An approximation of this kind damps the reflection of the shock wave. These boundary conditions are complemented by proper conditions for the turbulence model variables. The fluid was considered as ideal gas with proper constants (see Table 3). The quadrilateral multi-block grid with around 100 blocks and an O type block with a sufficiently stretched grid around the profile was generated by GridPro software. The mesh contained about 64 000 cells with $y^+ < 0.2$. Details of the cells around the leading edge and the trailing edge are shown in Fig. 14 and Fig. 15. According to experience gained with previous calculations (e.g. Louda at al. 2012), both meshes are fine enough to provide mesh-independent results.

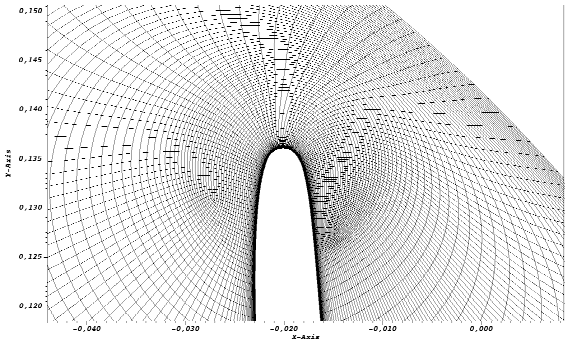

Figure 14: **Detail of the mesh around the leading edge (in-house code)**

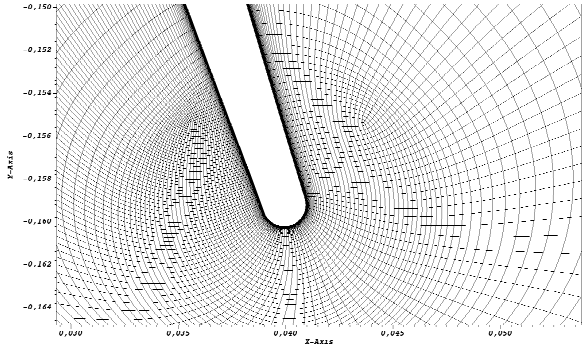

Figure 15: **Detail of the mesh around the trailing edge (in-house code)**

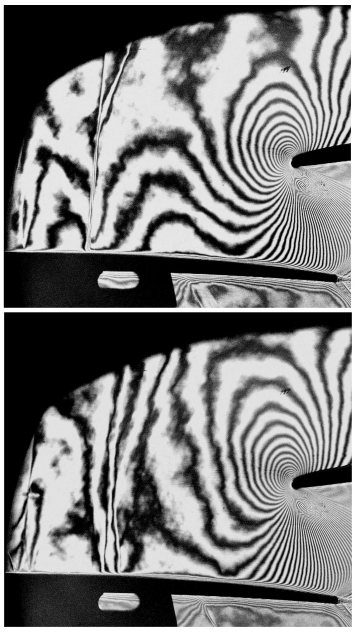

Figure 16: **Interferogram of the inlet flow field taken for the identical flow conditions: ι = +3°, M_1 = 0.933, M_{2is} = 1.612**

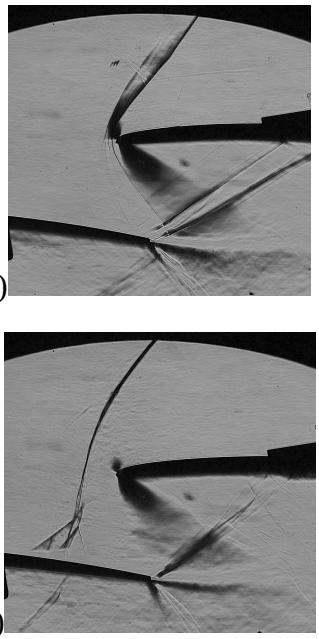

Figure 17: **Inlet shock wave, schlieren picture: a) M_1 = 1.555, M_{2is} = 1.713 b) M_1 = 1.562, M_{2is} = 1.592**

RESULTS AND DISCUSSION

In most measured regimes, the inlet flow field is characterized by the supersonic inlet velocity. Even in the case with positive incidence ι = +3°, the inlet Mach number is still so high that weak unsteady transonic flow field structures can be observed in the inlet flow field (Fig. 16). An inlet shock wave occurs in the flow field at supersonic inlet Mach numbers. The distance between the inlet shock wave and the leading edge depends not only on the inlet Mach number, but also on the back pressure. Two schlieren pictures taken at identical inlet Mach numbers and different isentropic exit Mach numbers are shown in Fig. 17. The corresponding distributions of the isentropic Mach number upstream and downstream the cascade along two pitches in the middle of the cascade are shown in Fig. 18 and Fig. 19. As the backpressure increases, the internal branch of the

inlet shock wave unbends and the whole shock wave shifts upstream the interblade channel. For constant sufficiently lower backpressure and for a rising inlet Mach number, the oblique internal branch of the inlet shock wave moves downstream into the interblade channel. A complex interaction with the boundary layer occurs on the pressure side of the adjacent profile, resulting in complicated viscous and dissipative structures. The boundary layer on the pressure side is laminar (see Straka et al. (2014)) upstream the interaction area. Unsteady behaviour is typical for this interaction. The point of this interaction moves towards the trailing edge with a further increase in the inlet velocity. Under certain pressure conditions, the shock wave even misses the surface of the adjacent blade and it interacts with the wake structures - see the examples in Fig. 20.

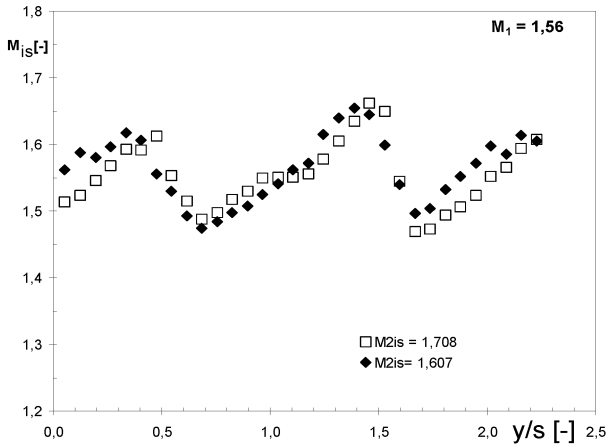

Figure 18: **Isentropic Mach number distribution along two pitches upstream the cascade for supersonic inlet velocity M_1 =1.56**

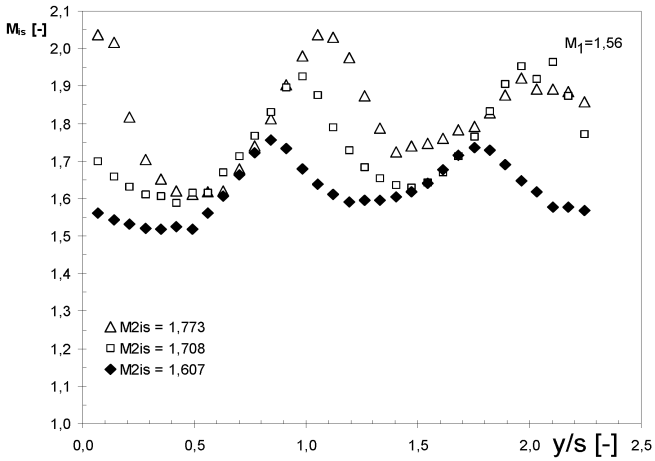

Figure 19: **Isentropic Mach number distribution along two pitches downstream the cascade for supersonic inlet velocity M_1 =1.56**

In most of the measured regimes, the flow field in the interblade channel is supersonic, with a small subsonic region around the leading edge. The sonic throat is missing. In the relatively small area of the interblade channel, very intense supersonic simple expansion takes place on the suction surface near the leading edge (see an example of the isentropic Mach number distribution in Fig. 22). The Mach number distribution along the suction side shows that this expansion area covers approximately 6% of the cascade chord x/b_{ax}. This expansion is followed by a region with practically constant high supersonic velocity ($M \sim 2$), which terminates in the region of the turbulent boundary layer - see Straka et al. (2014) - and the internal branch of the exit shock wave interaction on the profile suction side. This interaction takes place already in the exit part of the interblade channel (except for design regimes with very high backpressure) and it moves slightly downstream, depending on the drop in the backpressure. The interferograms show an increase in the thickness of the boundary layer downstream the interaction (see Fig. 21), and also the origin of a reflected shock wave, which afterwards interacts with wake downstream the adjacent profile.

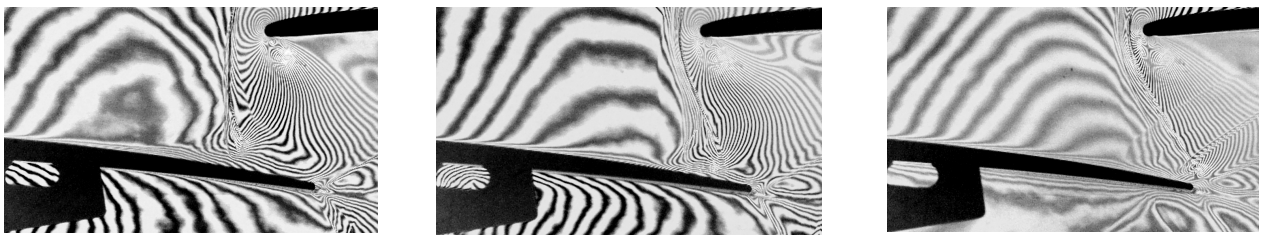

a) M_{2is} = 1.593 b) M_{2is} = 1.715 a) M_{2is} = 2.008

Figure 20: **Interaction of the internal branch of the inlet shock wave with the boundary layer on the pressure side of the adjacent profile, different back pressure, constant inlet Mach number $M_1 \sim 1.46$, interferograms**

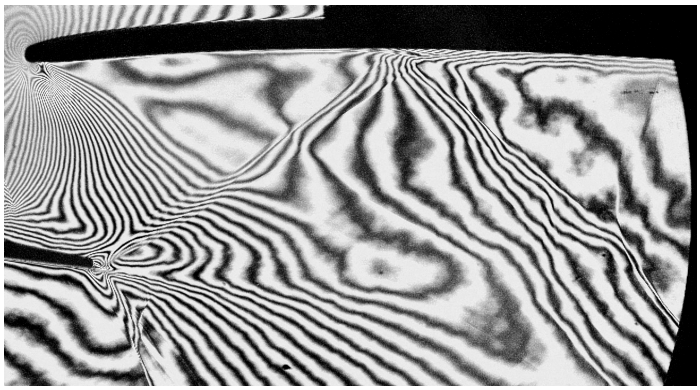

Figure 21: **An example of the interaction of the exit shock wave with the wake and boundary layer on the suction side of the neighbouring profile, interferogram, $M_1 = 1.502$, $M_{2is} = 1.598$**

The isentropic Mach number distribution along the rest of the suction side behind the interaction area is practically constant, and the value ranges from $M_{is} = 1.2$ to $M_{is} = 1.8$, depending on the inlet and exit flow conditions.

Figs 22 and 23 compare the distributions of the isentropic Mach number along the suction side and the pressure side of the profile. The first distribution is obtained from experiment, while the second distribution is obtained from CFD simulation (commercial code). The calculated flow field is completely turbulent, which ensures a more uncomplicated interaction of the boundary layer with the internal branch of the inlet shock wave on the pressure side of the profile (Fig. 25). By contrast, the test result (Fig. 24) shows a much more complex structure of the flow field, because the boundary layer on the pressure side is probably laminar up to the interaction area - see Straka et al. (2014). The impact of this complex interaction is that it suppresses the expansion area on the suction side of the neighbouring profile. Figure 30 gives an example of the inlet shock wave boundary layer interaction computed by the in-house code. The boundary layer upstream the interaction is also turbulent.

The isentropic Mach number on the pressure side reaches supersonic values in short rapid expansion downstream the stagnation point. This expansion continues till the trailing edge, but under a substantially smaller gradient. In several cases, the monotonous expansion is broken by the impact of the internal branch of the inlet shock wave close to the trailing edge.

The dependencies of the non-dimensional aerodynamic forces on the isentropic exit Mach number M_{2is} for a constant inlet isentropic Mach number (i.e. for constant incidences i) are evaluated from the interferograms. The aerodynamic force is solved by integrating the distribution of the static pressure along the pressure and suction sides in the peripheral direction. The data are related to the possible maximum of force $A.p_{01}$. The diagram in Fig. 27 shows clearly the dependence of the force on the incidence angle. The force decreases with increasing inlet Mach number (negative incidences) and, by contrast, it increases with decreasing inlet Mach number (positive angles), as expected. The values of the non-dimensional aerodynamic forces are small. In cases with extremely high inlet Mach number values, the aerodynamic force is even inverted.

The dependencies of the kinetic energy loss coefficient on the isentropic exit Mach number M_{2is} for different inlet velocities M_1 (or for different incidences) are shown in Fig. 28. Coefficient ζ is related to the value ζ^{nom}_{1200}, which was evaluated for the nominal operation condition specified for a 1200MW turbine. The curves clearly show an increase in the dissipation generated by the strengthening of the inlet shock wave when the inlet Mach number increases. The obvious trend of a decreasing kinetic energy loss coefficient for constant inlet parameters and an increasing isentropic exit Mach number shows the dependence of kinetic energy dissipation on the position of the internal branch of the interaction of the inlet shock wave with the neighbouring profile. The situation when the shock wave interacts with the boundary layer on the pressure side of the neighbouring profile is more dissipative than the state with the shock wave going through the near wake region downstream the blade. It is clarified by the comparison of the flow field structures in the interferograms in Fig. 20, together with the values of the energy loss coefficient.

Selected dependencies of the exit flow angle related to the exit flow angle evaluated for the nominal condition (a 1200MW turbine) for a constant incidence angle are plotted against the isentropic exit Mach number in the diagram in Fig. 29. The depicted data proves both the supersonic deflection of the flow for the range of inlet Mach numbers $1.0 < M_1 < 1.56$ and probably

its stagnation for $M_1 \geq 1.56$ (the changes in the exit flow angle taking place within the range of absolute uncertainties of the measuring equipment). The measured regimes with incidence $\iota = +3°$ (subsonic inlet velocity) exhibit an identical exit flow angle value up to $M_{2is} \approx 1.6$. Beyond this point, supersonic deflection takes place and the values of the exit flow angle decrease.

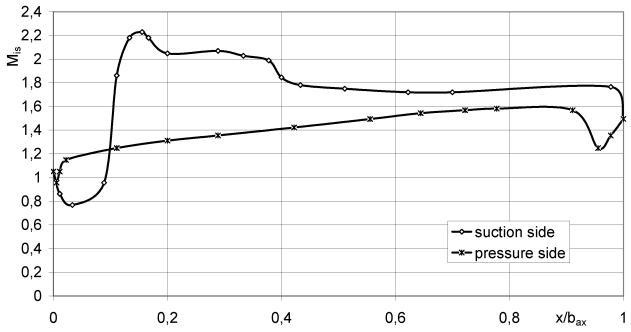

Figure 22: **Isentropic Mach number distribution along the profile for the nominal condition (turbine 1200 MW) M_1 =1.453, M_{2is} = 2.008 - interferometry**

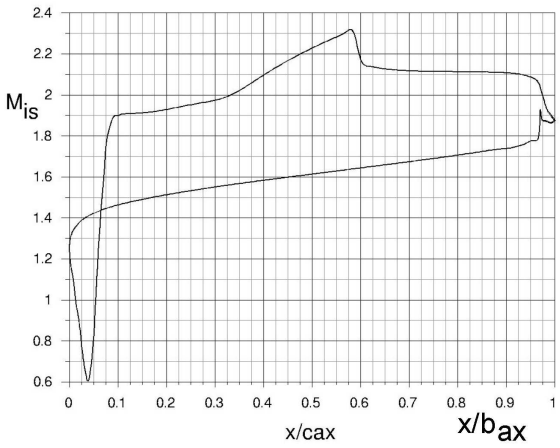

Figure 23: **Isentropic Mach number distribution along the profile for the nominal condition (turbine 1200 MW) M_1 =1.469, M_{2is} = 2.04 - CFD (commercial software)**

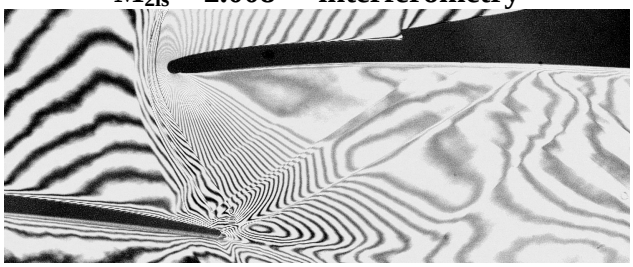

Figure 24: **Flow field in the interblade channel, interferogram M_1 =1.453, M_{2is} = 2.008 - interferometry**

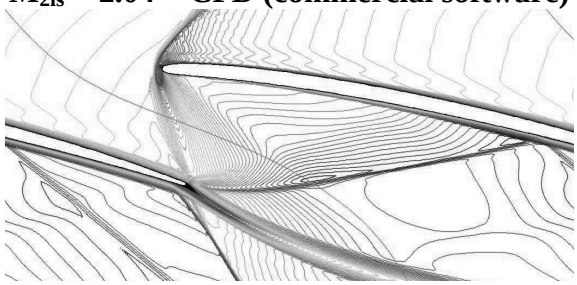

Figure 25: **Flow field in the interblade channel, interferogram M_1 =1.469, M_{2is} = 2.04 - CFD (commercial software)**

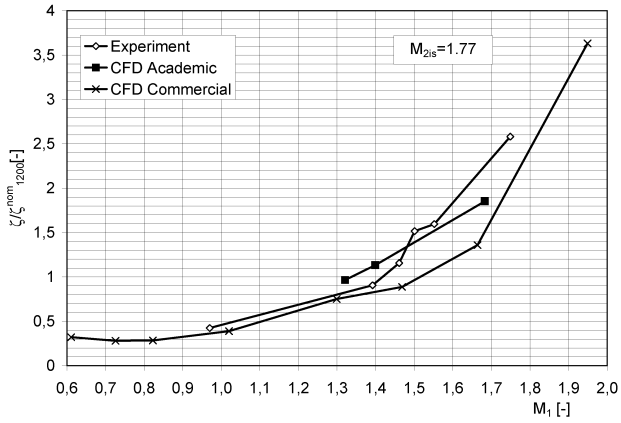

Figure 26: **Comparison of the kinetic energy loss obtained by experiment and by two different CFD calculations**

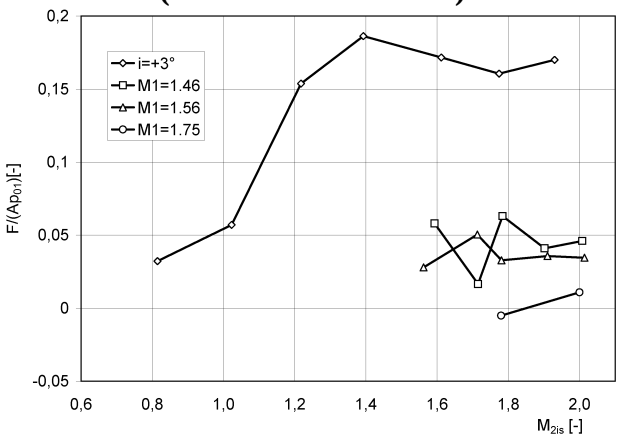

Figure 27: **Non-dimensional aerodynamic force**

The energy loss coefficient ζ^{nom}_{1200} is plotted against the inlet Mach number M_1 for M_{2is} = const (referring to nominal exit Mach number $M_{2is} \approx 1.77$) in Fig. 26. A comparison is made of the values obtained both experimentally and using numerical simulations. It can be seen that the CFD results correspond reasonably well with the data obtained experimentally. The dependence calculated by

the commercial code is rather more optimistic than the experimental results and also than the results of the other numerical simulation performed using the in-house code (a curve with three black points).

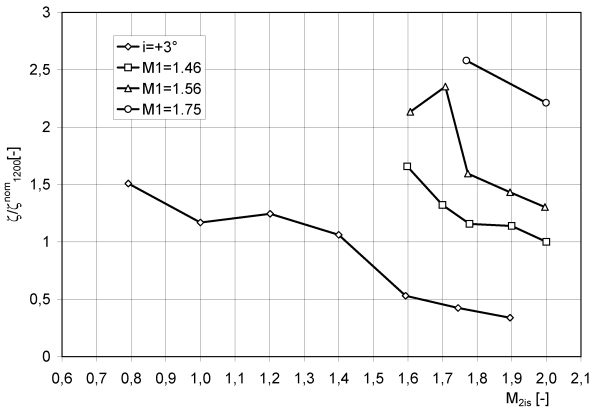

Figure 28: **Kinetic energy loss - experimental data**

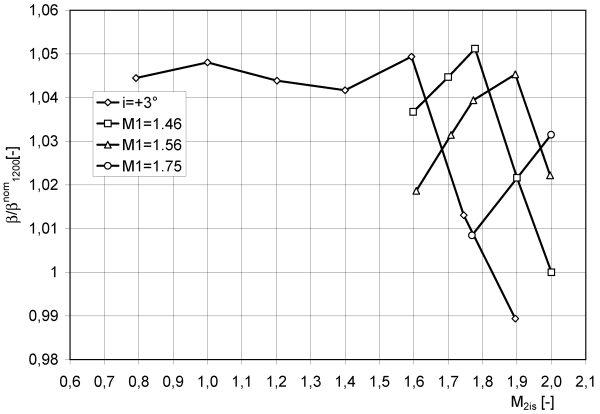

Figure 29: **Exit flow angle - experimental data**

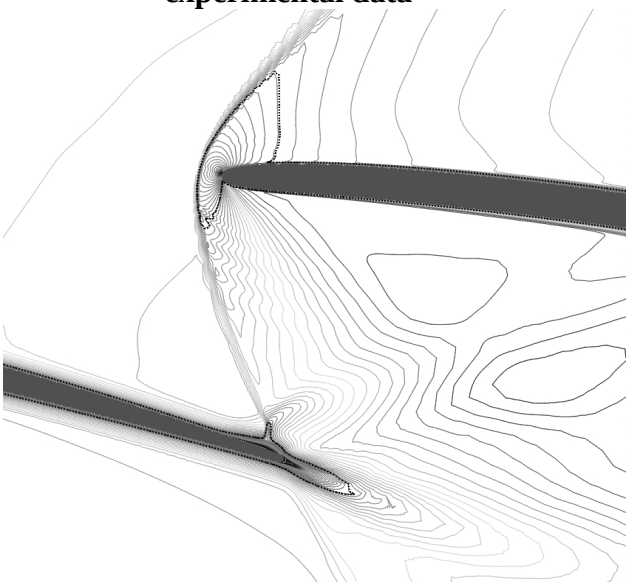

Figure 30: **Boundary layer and inlet shock wave interaction - isolines of Mach number, M_1 = 1.399, M_{2is} = 1.7, in-house code**

CONCLUSIONS

The experimental and numerical investigation of the flow past a blade cascade representing the tip section of long rotor titanium blading (54") has provided information on important cascade aerodynamic characteristics in a relatively wide range of flow regimes.

In a wide range of measured regimes, the flow field in the profile cascade is wholly supersonic, with the exception of a small closed subsonic area close to the leading edge. The changes in the inlet flow angle in the region of supersonic inlet Mach numbers are due to changes in the inlet Mach value. Correct inlet angle at supersonic regimes is set by setting corresponding inlet Mach number defined by the unique incidence rule.

The data obtained by applying mutually independent optical and pneumatic methods show that the intended operational condition for the 1200MW steam turbine is less dissipative than the second design condition determined for the 800MW steam turbine. The differences in the exit flow angle between the two design flow conditions are also important, and refer to air flow acceleration.

This experimental investigation of the tip sections of long rotor blades has provided not only unique and important knowledge about their aerodynamic quality, but also important information about the number of flow field phenomena occurring in complex flow fields of this type.

The comparisons of CFD and experimental results have shown that the advanced models used in the in-house code predicted loss coefficient values closer to the experimental data than the results predicted using the commercial code.

ACKNOWLEDGEMENTS

The authors would like to express their thanks to the Technology Agency of the Czech Republic, which supported this research under grant No. TA03020277. Institutional support RVO:61388998

is also gratefully acknowledged. The authors also thank DOOSAN ŠKODA POWER Co., Ltd., who made this research possible.

REFERENCES

Amecke, J., Šafařík, P.: *Data Reduction of the Wake Flow Measurements with Injection of an Other Gas.* Forschungsbericht DLR 95-32, Göttingen, 1995.

Aronowitz, S. et al.: *Technoscience and Cyberculture.* New York, London, Routledge, 1996.

Louda, P., Kozel, K., Příhoda, J.: *Numerical Modelling of Compressible Inviscid Flow and Viscous Flow in Turbine Cascades*. In: Algoritmy 2012, Proceedings of Contributed Papers and Posters., p. 301-310., Bratislava, 2012.

Luxa, M., Rudas, B., Synáč, J., Šafařík, P., Šimurda, D.: *Experimental Technique for Setup of Supersonic Inlet Flow in a Profile Blade Cascade.* In: The Application of Experimental and Numerical Methods in Fluid Mechanics and Energy 2014, pp. 149 - 152, Žilina, 2014.

Matějka, M., Luxa, M., Šimurda, D.: *Test Section for Low Turning Angle Cascade Testing*. Research report IT CAS No. 1502/13, Prague, 2013 (in Czech).

Šafařík, P., Luxa, M.: *Using Optical Methods in High-Speed Aerodynamic Research*. In: Measurement Techniques in Turbomachinery XX, pp. 1-7, Firenze, 2000.

Senoo, S.: *Development of Design Method for Supersonic Turbine Aerofoils near the Tip of Long Blades in Steam Turbines, Part 1: Overall Configuration*. In: Proceedings of ASME Turbo Expo 2012, GT2012-68218, Copenhagen, 2012.

Šimurda, D., Luxa, M., Šafařík, P., Synáč, J., Rudas B.: *Measurements on Supersonic Turbine Cascades - Methodical Approach*. In: The XXII Symposium on Measuring Techniques in Turbomachinery, Transonic and Supersonic Flow in Cascades and Turbomachines, Lyon, 2014

Starken, H.: *Utilization of Linear Cascade Experiments in Turbomachine Design Development*. DFVLR Report No.IB-325-19-86, Cologne, 1986.

Straka, P., Stodůlka, J., Příhoda, J.: *Modelling of Flow through the Tip Section Turbine Blade Cascade with a Supersonic Inlet* (in Czech). In:Turbostroje 2014, Pilsen, 2014.